Journal of Sound and Vibration 331 (2012) 1469–1482

Contents lists available at SciVerse ScienceDirect

Journal of Sound and Vibration

journal homepage: www.elsevier.com/locate/jsvi

Active suppression of panel flutter with piezoelectric actuators using eigenvector orientation method

Zhanxi Wang [a,b], Xiansheng Qin [a], Henry T.Y. Yang [b,*]

[a] Department of Industrial Engineering, Northwest Polytechnical University, Xi'an 710072, China
[b] Department of Mechanical Engineering, University of California, Santa Barbara, CA 93106, USA

ARTICLE INFO

Article history:
Received 30 March 2011
Received in revised form
8 November 2011
Accepted 18 November 2011
Handling Editor: D.J Wagg
Available online 15 December 2011

ABSTRACT

This paper examines the use of eigenvector orientation method to detect the onset of subsonic and supersonic flutter of panels modeled by finite elements. The accuracy of the eigenvector orientation method for prediction of the flutter boundary (indicated by a gradual loss of orthogonality between two eigenvectors) is demonstrated by using the examples of a swept-back cantilever plate model at subsonic speed and a simply supported plate model at supersonic speed. Piezoelectric layers are assumed to be bonded to the top and bottom surfaces of the simply supported plate in order to provide bending moments to control motions of each finite element. An approach of optimal control design is presented to actively suppress the possible flutter based on linear quadratic regulator theory and the nonlinear modal equations of motions. To illustrate the applicability and effectiveness of using the piezoelectric layers as controllers, several cases are studied and presented. The effects of varying locations of control moments are studied so as to fulfill the objective of adjusting the flutter speed to be within a desirable range. The results illustrate that the control moment manipulation can offset the flutter occurrence and additionally generate a lead time for possibly executing flutter control.

1. Introduction

Flutter has been considered as one of the most destructive causes of failure in aircrafts, missiles and various flight vehicles [1–4]. In the past seven decades, this phenomenon has continuously motivated researchers and designers to use a variety of methods to analyze, predict, and most importantly, avoid the flutter. The predominant dynamic flutter instability needs to be investigated for the design optimization of most flight vehicles. There are several methods used to predict the onset of flutter instability in aeroelastic design optimization. One popular approach is to use finite elements in the form of beam, plate, and shell elements to take advantage of their versatility in geometry, boundary, and material modeling [5]. The finite element method was first applied to the problem of panel flutter by Olson [6] in 1967. Olson, in Ref. [7], extended the finite element method to three dimensional applications by using the concept of formulating an aerodynamic matrix in addition to the stiffness and mass matrices of rectangular and triangular plate bending elements, and predicted a definition that flutter occurs when the lowest two vibration modes coalesce. Later, Yang applied the finite element method to the nonlinear panel flutter in supersonic potential flow [8–10]. In a more recent work by Afolabi,

* Corresponding author.
E-mail address: henry.yang@chancellor.ucsb.edu (H.T.Y. Yang).

0022-460X/$ - see front matter © 2011 Elsevier Ltd. All rights reserved.
doi:10.1016/j.jsv.2011.11.015

Pidaparti and Yang [11–13], an alternative approach based on the eigenvector orientation method was developed to detect the onset of flutter for the isotropic and composite plate.

Active control of flutter suppression is an important component of aircraft design. A significant amount of research has been carried out on flutter suppression by the use of advanced materials. Among these materials, piezoelectric materials have drawn attention as possible actuation mechanisms for flutter prevention systems because of their simple material properties and fast response time. Scott and Weisshaar [14] were among the earliest to perform active suppression control on linear panel flutter with piezoelectric material using the Ritz method. Zhou et al. [15] presented a finite element formulation for the nonlinear flutter suppression of an isotropic panel under uniform thermal loading by using the modal reduction scheme and feedback linear control. Forster and Yang [16] used piezoelectric actuators to control supersonic flutter of wing boxes. Sebastijanovic et al. [17] used the eigenvector orientation method and piezoelectric layers to shift flutter speeds of a simple finite element with beam model. In the study, they generate a 'lead-time' by tracking the eigenvectors and the angle between them as it gradually approaches zero. This potential lead-time may provide more room for the study of a more timely and effective control and prevention of flutter that flight vehicles with plate and shell structures might experience.

In this study, the application realm of eigenvector orientation approach is extended from the wide-beam model to the wing panel model with the examples of a cantilever plate in subsonic flow and a simply supported plate in supersonic flow. The aeroelastic formulation of the plates has been derived by using the finite element method and panel aerodynamic theory. To further illustrate the validity and suitability of the developed methods, some results with flutter speeds and mode shapes are verified by comparing the present results with those given in Refs. [11,18]. Piezoelectric layers are used as actuators that produce counter balancing bending moments at each controlled subcomponent to suppress the flutter and shift the flutter speed. The linear quadratic regulator controller design is developed for various attempts to change piezoelectric actuators placements. To illustrate the usefulness and applicability of the piezoelectric actuators, several specific panel examples with different locations of piezoelectric layers are studied and provided.

2. Structure model

The first example studied is a swept-back cantilever plate in subsonic flow, similar to that used in Ref. [18]. This plate is assumed to have a span of 15.75 in., a chord of 7.87 in., a thickness of 0.045 in. and a swept-back angle of 30°, respectively. In the current illustrative example, a mesh of 6×7 triangular plate bending elements, with each element possessing three degrees of freedom at each of the three corner node (transverse displacement and derivatives w, w_x, w_y) [19], is used to model the cantilever plate as shown in Fig. 1a. The second example is a simply supported rectangular plate by assumed stringers and ribs in supersonic flow. Both length and width of this plate are assumed to be 10 in., and the thickness is assumed to be 0.1 in. In this example, a mesh of 4×4 rectangular plate bending elements, with each element possessing four degrees of freedom at each of the four corner node (transverse displacement and derivatives w,w_x, w_y, w_{xy}) [20], is used to model the simply supported plate as shown in Fig. 1b. It must be noted that the 16 degrees of freedom conforming rectangular element has long been shown as the most effective rectangular plate bending element [21]. However, it cannot be used to model quadrilateral plate with corner angles other than 90° such as those in a swept plate. Because of this limitation, the current swept plate is modeled using 9 degrees of freedom triangular elements in Example 1.

The top and bottom layers of the rectangular plate are symmetrically bonded with piezoelectric actuators, which are applied to produce control bending moments, as shown in Fig. 1c. The materials properties of the base plates and piezoelectric actuators are presented in Table 1. Because the thickness of these piezoelectric actuators are assumed to be very small as compared with the thickness of the plates, the structure changes due to these piezoelectric layers can be considered negligible.

In this study, piezoelectric patches are assumed to be applied as bimorph actuator on the top and bottom part of each panel element independently. This allows each element to experience a positively or negatively defined bending moment by having the top layer in compression and the bottom layer in tension, or vice versa. As shown in Fig. 2, only three simple cases are considered for illustrative purpose. Depending on the direction of airflow, controllers are designed to modify the system stiffness matrix by assuming that control bending moments are applied to all the 16 elements, to the eight end elements, or to the eight interior elements.

3. Finite element formulation

The linear constitutive equations of the piezoelectric material can be written as [22]

$$\boldsymbol{\sigma} = \mathbf{c}^E \boldsymbol{\varepsilon} - \mathbf{e}^T E, \quad \mathbf{D} = e\boldsymbol{\varepsilon} + \boldsymbol{\epsilon}^S \mathbf{E} \tag{1}$$

where $\mathbf{c}^E$ is the elastic stiffness matrix, superscript T denotes transpose, $\mathbf{E}$ is the electric field vector, $\mathbf{D}$ is the electric displacement vector, $\boldsymbol{\epsilon}^S$ is the dielectric constant matrix, and e is the piezo stress/charge constant.

As stated earlier, the plates are modeled by using the three-corner-node triangular plate elements and the four-corner-node rectangular plate elements [21]. There are three bending degrees of freedom (w, w_x, w_y) at each node of the triangular element, four bending degrees of freedom (w, w_x, w_y, w_{xy}) at each node of the rectangular element, and two electrical

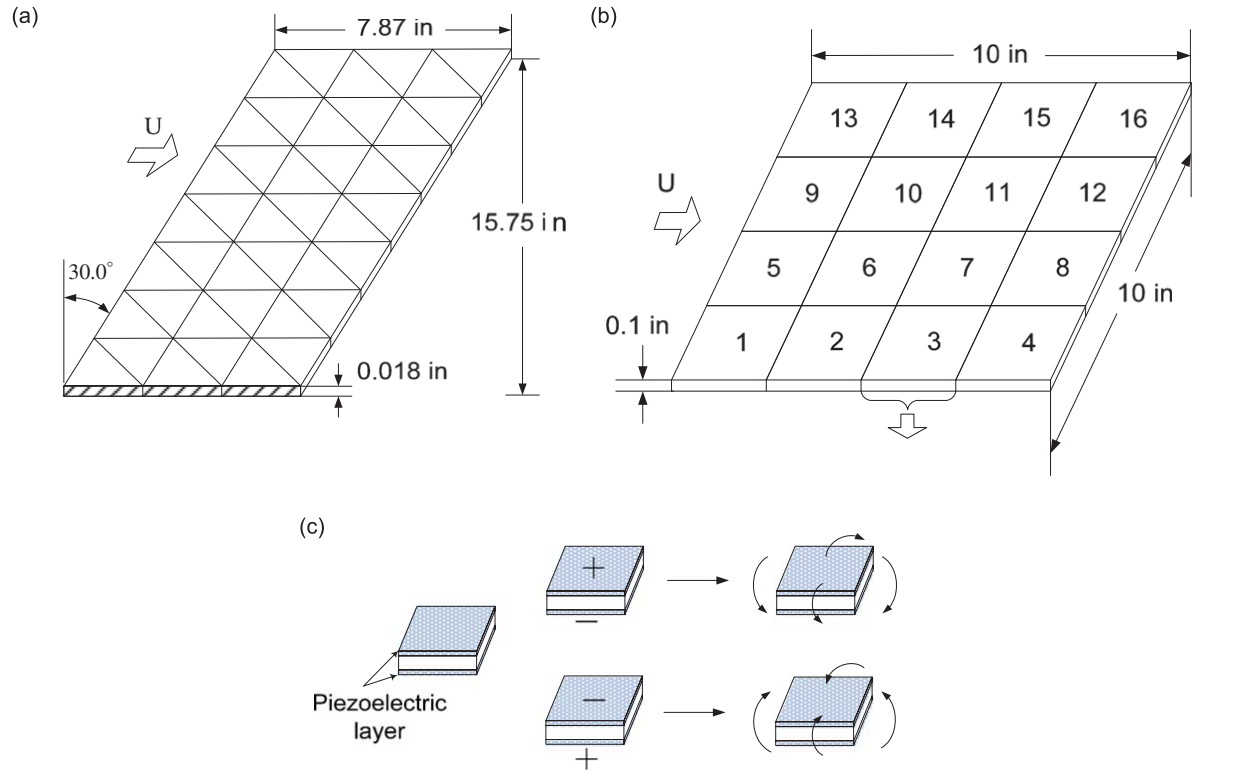

Fig. 1. (a) Configuration of swept-back cantilever plate, (b) configuration of simply supported plate and (c) moments created by piezoelectric layers for each elements of (b).

Table 1
Material properties of the plates and piezoelectric actuators.

Material properties	Swept-back cantilever plate	Simply supported rectangular plate	Piezoelectric actuators
Young's modulus,10^6 psi	10.0	10.0	9.135
Density (lb/in.^{3})	0.1	0.1	0.275
Poisson's ratio	0.3	0.3	0.35
Tensile strength (ksi)	65.0	65.0	9.135
Compressive strength (ksi)	65.0	65.0	75.4
Piezo constant (m/V)	–	–	-166×10^{-12}

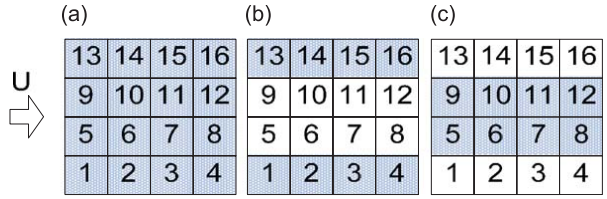

Fig. 2. Placement of the piezoelectric actuators (in shaded elements) in the three illustrated cases: (a) all 16 elements, (b) eight end elements, and (c) eight interior elements.

degrees of freedom (ϕ) per piezoelectric layer per element. The related vectors are given as

$$\mathbf{w}_{e1}=\{w_1,w_{1x},w_{1y},w_2,w_{2x},w_{2y},w_3,w_{3x},w_{3y}\}^T,$$

$$\mathbf{w}_{e2}=\{w_1,w_{1x},w_{1y},w_{1xy},w_2,w_{2x},w_{2y},w_{2xy},w_3,w_{3x},w_{3y},w_{3xy},w_4,w_{4x},w_{4y},w_{4xy}\}^T,$$

$$\boldsymbol{\varphi}=\{\phi_{11},\phi_{12},\phi_{21},\phi_{22},\phi_{31},\phi_{32},\ldots,\phi_{n1},\phi_{n2}\}, \tag{2}$$

where $\mathbf{w}_{e1}$ and $\mathbf{w}_{e2}$ are the nodal displacement vectors of triangular plate element and rectangular plate element, respectively, $\boldsymbol{\varphi}$ is the plate electric potential vector, and n is the number of piezoelectric layers.

For low Mach number subsonic flow ($M_\infty \ll 1$), the self-induced aerodynamic pressure is approximately given as [2,23]

$$p_{a1} = 2A_0 q_a \left(\frac{\partial^2 w}{\partial x^2} + \frac{2}{U_\infty} \frac{\partial^2 w}{\partial x \partial t} + \frac{1}{U_\infty^2} \frac{\partial^2 w}{\partial t^2} \right) \tag{3}$$

where $A_0 = b/\pi \int_{-x/a}^{1-(x/a)} \ln|y/b|\, dy$ is the coefficient of aerodynamic pressure for subsonic flow, $q_a = \rho_a U_\infty^2/2$ is the free stream dynamic pressure, ρ_a is the air mass density, U_∞ is the free stream airflow speed and w is the transverse displacement of panel.

The aerodynamic pressure parameter is defined as

$$\lambda_1 = 2A_0 q_a \tag{4}$$

For high Mach number supersonic flow ($\sqrt{2} < M_\infty < 5$), the first-order piston theory is suitably used to describe the aerodynamic pressure loads acting on the plate [2,7,9]. The aerodynamic pressure can be expressed as

$$p_{a2} = \frac{2q_a}{\sqrt{\left(M_\infty^2 - 1\right)}} \left(\frac{\partial w}{\partial x} + \frac{1}{U_\infty} \frac{M_\infty^2 - 2}{M_\infty^2 - 1} \frac{\partial w}{\partial t} \right) \tag{5}$$

where the aerodynamic pressure parameter is defined as

$$\lambda_2 = \frac{2q_a}{\sqrt{(M_\infty^2 - 1)}} \tag{6}$$

By using the above equations, the element matrices can be obtained. The detailed derivation of these element matrices can be found in Refs. [7,9]. We can derive the equation of motion for an actively controlled finite element plate subjected to aerodynamic loads as follows:

$$\mathbf{M}_e \ddot{\mathbf{W}}_e + \mathbf{C}_e \dot{\mathbf{W}}_e + (\mathbf{K}_e + \mathbf{A}_e + \mathbf{K}_1 + \mathbf{K}_2 - \mathbf{K}_{w\varphi} \mathbf{K}_{\varphi\varphi}^{-1} \mathbf{K}_{w\varphi}) \mathbf{W}_e = \mathbf{K}_{w\varphi} \mathbf{V}_a \tag{7}$$

where $\mathbf{M}_e$, $\mathbf{C}_e$, $\mathbf{K}_e$ are the mass, damping, and stiffness matrices, $\mathbf{A}_e$ is the aerodynamic matrix, $\mathbf{K}_1$ and $\mathbf{K}_2$ are the first-order nonlinear stiffness and second-order nonlinear stiffness matrices which depend linearly and quadratically on the displacements, respectively, $\mathbf{K}_{w\varphi}$ is the elastic–electric coupling stiffness matrix, $\mathbf{K}_{\varphi\varphi}$ is the dielectric stiffness matrix, W_e is the vector of node displacements, and $\mathbf{V}_a$ is the vector of applied voltages. It should be noted that Eq. (7) can be applicable for both subsonic and supersonic situation, but their aerodynamics matrixes are different, and can be deduced from Eqs. (3) and (5) by using the principle of virtual work, respectively.

Since the linear panel flutter is unstable when λ is above a critical aerodynamic pressure parameter, indicated as λ_{cr}, whereas the nonlinear panel flutter is a stable limit-cycle oscillation, we can neglect the nonlinear stiffness matrixes in the suppression of panel flutter. By assembling the element matrices and ignoring the nonlinear terms, the equation of motion for the entire structure can be written as

$$\mathbf{M}\ddot{\mathbf{W}} + \mathbf{C}\dot{\mathbf{W}} + (\mathbf{K} + \lambda \mathbf{A})\mathbf{W} = \mathbf{U} \tag{8}$$

where $\mathbf{M}$, $\mathbf{C}$, $\mathbf{K}$, $\mathbf{A}$ are the mass, damping, stiffness and aerodynamic matrixes by assembling the element matrixes and introducing the boundary conditions, λ is the aerodynamic pressure parameter and can be found in Eqs. (4) and (6) for subsonic and supersonic flow, $\mathbf{U} = \mathbf{K}_{w\varphi} \mathbf{V}_a + \mathbf{K}_{w\varphi} \mathbf{K}_{\varphi\varphi}^{-1} \mathbf{K}_{w\varphi} \mathbf{W}$ is the control moments in the controller design instead of $\mathbf{V}_a$ for simplicity.

When $\lambda = 0$, the generalized eigenvalues are real and positive definite. As λ increases from zero, the eigenvalues of two lowest modes will usually approach each other and coalesce at a critical value λ_{cr} and become complex conjugate pairs. The corresponding eigenvectors will lose their orthogonality and become complex. Hence the onset of flutter can be predicted by using the eigenvector orientation method to track the angle between the two eigenvectors. Here, The angle between two eigenvectors can be derived from their scalar product [11]. For two real vectors, the angle is the arc cosine

$$\theta = \cos^{-1} \left(\frac{\mathbf{v}_1 \cdot \mathbf{v}_2}{\|\mathbf{v}_1\| \|\mathbf{v}_2\|} \right) \tag{9}$$

The angle between two complex vectors is calculated by mapping a complex vector into a real vector by grouping the imaginary components after the real components, so that

$$\theta = \cos^{-1} \left(\frac{\bar{\mathbf{v}}_1 \cdot \mathbf{v}_2}{\|\bar{\mathbf{v}}_1\| \|\mathbf{v}_2\|} \right) \tag{10}$$

where an overbar denotes complex conjugation.

4. Optimal control design

Based on the reduced model of entire structure, an output feedback controller can be designed by using the linear quadratic regulator theory [24]. Introducing the state-space variables

$$\mathbf{x}=[\mathbf{W}_i\ \dot{\mathbf{W}}_i]^T,\quad \mathbf{u}=[\mathbf{0}\ \mathbf{U}]^T \tag{11}$$

The second-order nonlinear coupled-modal equation given by Eq. (8) can be converted to a first-order state space form as

$$\dot{\mathbf{x}}=\mathbf{S}\cdot\mathbf{x}+\mathbf{B}\cdot\mathbf{u} \tag{12}$$

where $\mathbf{S}$ is the system matrix, and $\mathbf{B}$ is the control influence coefficient matrix, determined according to the actuator configuration, which are given by

$$\mathbf{S}=\begin{bmatrix} 0 & \mathbf{I} \\ -\mathbf{M}^{-1}(\mathbf{K}+\lambda\mathbf{A}) & -\mathbf{M}^{-1}\mathbf{C}\end{bmatrix},$$
$$\mathbf{B}=\begin{bmatrix}\mathbf{0} & \mathbf{M}^{-1}\mathbf{E}\end{bmatrix}^T \tag{13}$$

where $\mathbf{E}$ is determined according to the actuator configuration, for example, $\mathbf{E}=\mathbf{I}$ when all 16 elements are controlled.

The linear quadratic performance index for optimal control can be formulated as

$$J=\int_0^\infty(\mathbf{x}^T\cdot\mathbf{Q}\cdot\mathbf{x}+\mathbf{u}^T\cdot\mathbf{R}\cdot\mathbf{u})d\tau \tag{14}$$

where $\mathbf{Q}$ is a positive semidefinite penalty weighting matrix, and $\mathbf{R}$ is a positive definite control weighting matrix. In this study, $\mathbf{Q}=q\times\mathbf{I}$ and $\mathbf{R}=r\times\mathbf{I}$, where r is identity, and q is an appropriately chosen constant.

From the optimal control theory, the optimal linear feedback control force vector can be written as

$$\mathbf{u}=-\mathbf{R}^{-1}\cdot\mathbf{B}^T\cdot\mathbf{P}\cdot\mathbf{x} \tag{15}$$

where $\mathbf{P}$ is a positive so-called Riccati matrix obtained by solving the following algebraic Riccati equation:

$$\mathbf{S}^T\cdot\mathbf{P}+\mathbf{P}\cdot\mathbf{S}-\mathbf{P}\cdot\mathbf{B}\cdot\mathbf{R}^{-1}\cdot\mathbf{B}^T\cdot\mathbf{P}+\mathbf{Q}=0 \tag{16}$$

From Eq. (15), the feedback gain matrix for this control design is defined as

$$\mathbf{G}=\mathbf{R}^{-1}\cdot\mathbf{B}^T\cdot\mathbf{P} \tag{17}$$

Substituting Eq. (15) into Eq. (12), we obtain

$$\dot{\mathbf{x}}=(\mathbf{S}-\mathbf{B}\cdot\mathbf{G})\cdot\mathbf{x}=\mathbf{S}_c\cdot\mathbf{x} \tag{18}$$

where $\mathbf{S}_c=\mathbf{S}-\mathbf{B}\cdot\mathbf{G}$ is the "closed-loop" dynamics matrix, and the system coefficient change induced by the feedback control is

$$\Delta\mathbf{S}=\mathbf{B}\cdot\mathbf{G} \tag{19}$$

This system matrix change represents the effect that would be created by applied control moments which are produced by piezoelectric layers. By adding the change to Eq. (8), the controller is able to restabilize the system. The block diagram representation of the controller is illustrated in Fig. 3.

It should be noted that the design process requires a specific airspeed and altitude condition, which mean that each controller is based on the structural model with a design specific aerodynamic pressure, indicated as λ_d. After each design, the maximum control output is measured when the system is perturbed by exciting the piezoelectric actuators using an impulsive input. The value of dynamic pressure is increased and the design process for different weighting matrices is carried out. This process is repeated up to a certain value beyond which the linear quadratic regulator controller could not stabilize the system without saturation.

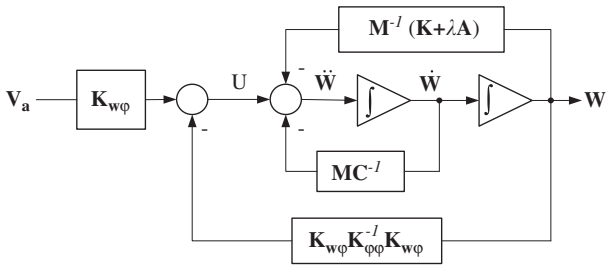

Fig. 3. Block diagram for linear quadratic regulator feedback controller design.

5. Numerical simulations and results

Computer programs are developed and tested for the present isotropic plate finite element formulations and their application to subsonic and supersonic panel flutter analysis. Firstly, the computed results of the natural frequencies and mode shapes of the examples using the present finite element models are obtained from the presently developed computer programs, and the results are compared with the analytical and experimental solution as given in Refs. [11,18]; Secondly, both the present eigenvector orientation method and the method of coalescence of eigenvalues are used to detect the onset of flutter; finally, the piezoelectric layer actuators are applied to the second test model, and the actual effect is analyzed and discussed by changing the location of piezoelectric layers.

5.1. Swept-back cantilever plate under subsonic flow

This example is used to verify the validity of the present finite element and eigenvector orientation methods. As a first step, a free vibration analysis is performed for this cantilever plate model by neglecting the damping and aerodynamic effect. The natural frequencies are first obtained and compared with those values presented by Han et al. [18]. The material properties and dimensions used for this comparison are the same, as shown in Table 1 and Fig. 1a. The details of comparison can be found in Table 2. It is seen that the first five natural frequencies obtained by the present 6×7 triangular elements are in good agreement with those obtained in Ref. [18] by using both the experimental method and the 20×40 four-node elements.

By using the coalescence of eigenvalues method and the eigenvector orientation method, the flutter predictions are obtained when subjected to subsonic flow. The reference Mach number is assumed to be 0.05 (35.3 m/h at sea level), and the structural damping is not taken into account. Fig. 4a shows the variation of frequencies for the two fundamental modes as a function of the aerodynamics pressure parameter for this model. It can be seen that when the aerodynamic pressure parameter reaches 5.6, the natural frequencies of modes 1 and 2 coalesce and exhibit complex eigenvectors, which means that modes 1 and 2 are participating in the dynamics in such a way as to give rise to a flutter condition. Fig. 4b shows the variation of the angle between the two eigenvectors as a function of the aerodynamic pressure parameter. It can be seen that the angle between the two eigenvectors drops from 90° to zero as the plate approaches the flutter condition at $\lambda_{cr}=5.6$. This phenomenon indicates that the eigenvectors initially are oriented orthogonally but gradually lose their orthogonality as the aerodynamic pressure parameter is varied.

Fig. 5 shows the first two mode shapes of lifting surface at three stages with different values of aerodynamic pressure parameter. During the free vibration at $\lambda_1=0$, it can be seen that the first mode is dominated by a bending mode, whereas the second mode is mainly dominated by a torsional mode. As aerodynamic pressure parameter increased from zero, the

Table 2
Natural frequencies of the swept-back cantilever plate.

Mode number	Ref. [18]		Present analysis (6×7 three-node elements) (Hz)
	Experiment (Hz)	20×40 four-node elements model (Hz)	
1	2.03	2.13	2.17
2	10.9	10.4	10.3
3	14.5	14.3	14.8
4	31.2	29.6	33.3
5	43.9	41.7	41.8

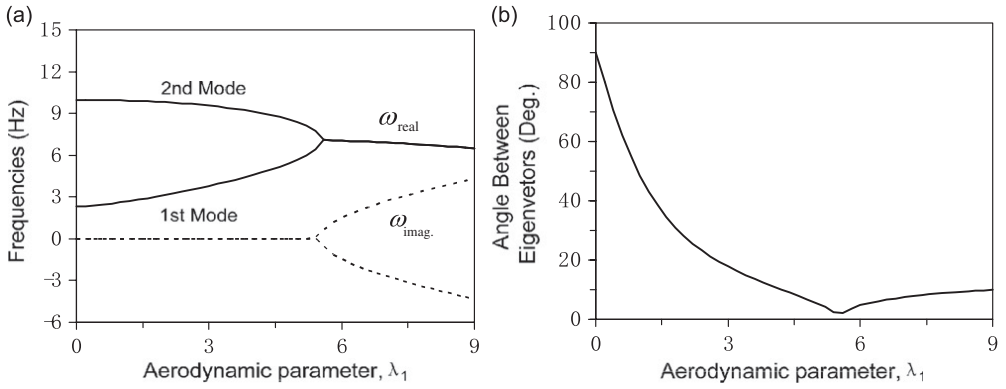

Fig. 4. Flutter prediction of the swept-back cantilever plate by using both methods: (a) coalescence of eigenvalues and (b) eigenvector orientation.

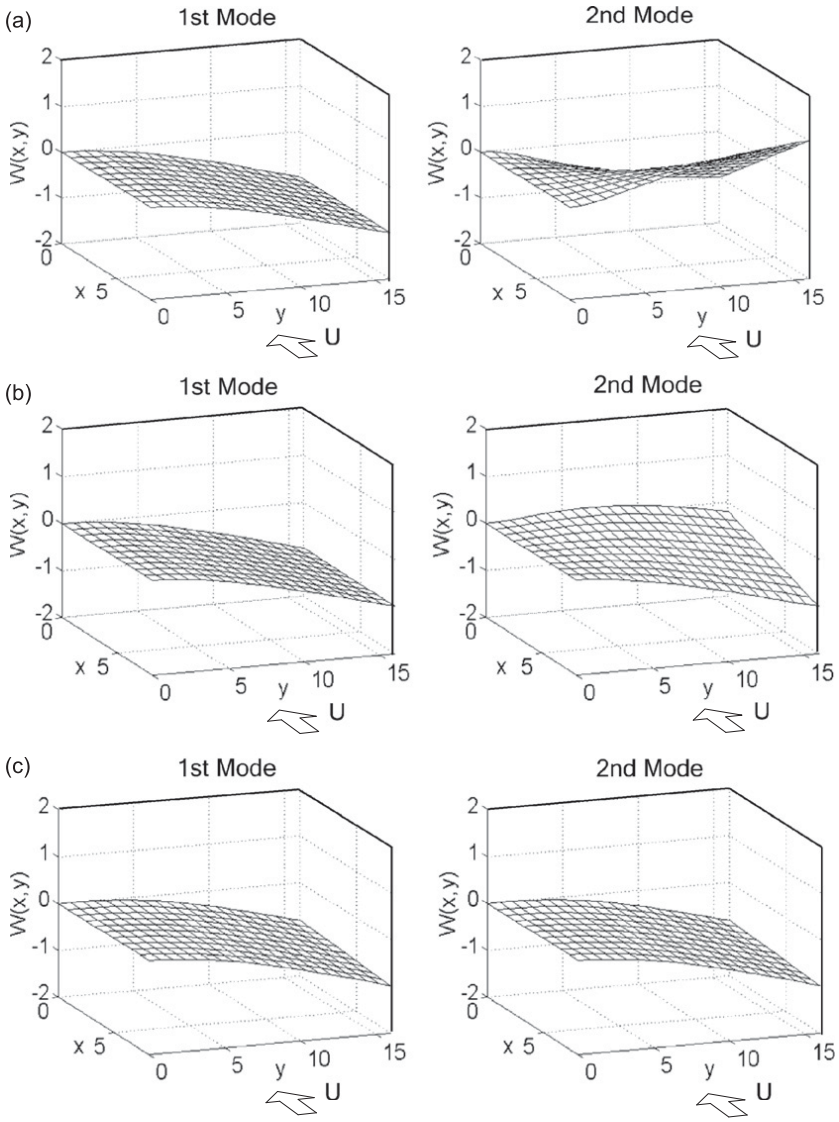

Fig. 5. Mode shapes of lifting surface at three stages: (a) free vibration, (b) aerodynamic pressure parameter $\lambda_1=4$ and (c) coalesce of lowest two modes at $\lambda_{cr}=5.6$.

Table 3
The comparison of the flutter speed and frequency.

	Ref. [18]		Present analysis (eigenvector orientation method)
	Experiment	V-g method	
Flutter speed (m/s)	17.1	15.1	16.8
Flutter frequency (Hz)	7.2	8.2	7.1

first mode keeps the original modality while the second mode gradually loses its torsion dominant modality under the effect of airflow. Finally, the lowest two modes become similar at $\lambda_{cr}=5.6$, indicating the coalesce and the onset of flutter.

Both the coalescence of eigenvalues method and the eigenvector orientation method are used to find the flutter frequency of 7.1 Hz and the flutter aerodynamic pressure parameter of 5.6, which can be converted to the flutter speed 16.8 m/s by Eq. (4). Table 3 compares the flutter boundaries with Ref. [18]. It can be seen that the present results show reasonably good agreement with the experimental and analytical results, which indicates that the current finite element model and eigenvector orientation method can predict the onset of flutter for the swept-back cantilever plate under subsonic flow with reasonable accuracy. It should be noted that a distinct characteristic of the eigenvector orientation

method is that it can predict the flutter condition by tracking the angle between the two eigenvectors and its deviation from 90°. Thus, for a real-time flutter control process and design, in which the response time is critical, the eigenvector orientation method has its practical value because it can be easily monitored.

5.2. Simply supported plate under supersonic flow

To further illustrate the application of eigenvector orientation method in the flutter process and design, the example of a simply supported plate bonded with piezoelectric layers under supersonic flow is considered. This model is analyzed to find combinations of control parameters that would result in offsetting flutter to a higher speed. The structural model can be seen in Fig. 1b. As a first step, the flutter prediction of uncontrolled case is analyzed by using both methods: the coalescence of eigenvalues, and the eigenvector orientation. As shown in Fig. 6a, flutter occurs as the eigenvalues of the two lowest modes coalesce around a critical value of aerodynamic pressure at $\lambda_{cr}=480$. This corresponds to the flutter condition when the angle between the two eigenvectors drops to zero and yield the same value at $\lambda_{cr}=480$ as shown in Fig. 6b.

To further observe the control effect, a set of examples are considered by changing locations for the application of piezoelectric layers. For each example, different controllers are obtained by fixing the control weighting matrix **R** while varying the penalty weighting matrix **Q**, and each controller is designed based on a model with a specific aerodynamic pressure parameter λ_d. So the actual control parameters are the constant q and design aerodynamic pressure parameter λ_d in the controller design procedure.

5.2.1. Case 1: Applying control moments on all 16 elements

When the control bending elements are applied on all 16 elements, the flutter speed can be both decreased and increased depending on the control parameters q and λ_d. This concept is illustrated in Fig. 7. It can be seen that a series of combinations of control parameters q and λ_d are used to obtain seven critical flutter speeds varying from $\lambda_{cr}=200$ to 840 including the uncontrolled case of $\lambda_{cr}=480$.

To be more specific numerically, all critical flutter speeds and the corresponding control parameters q and λ_d are listed in Table 4. It is noticed that for $\lambda_d=0$, flutter speed seems to increase as the control parameter q decreases. Because the controller is only affected by the control parameter q at $\lambda_d=0$, the stiffness of the structure is actually decreased and the

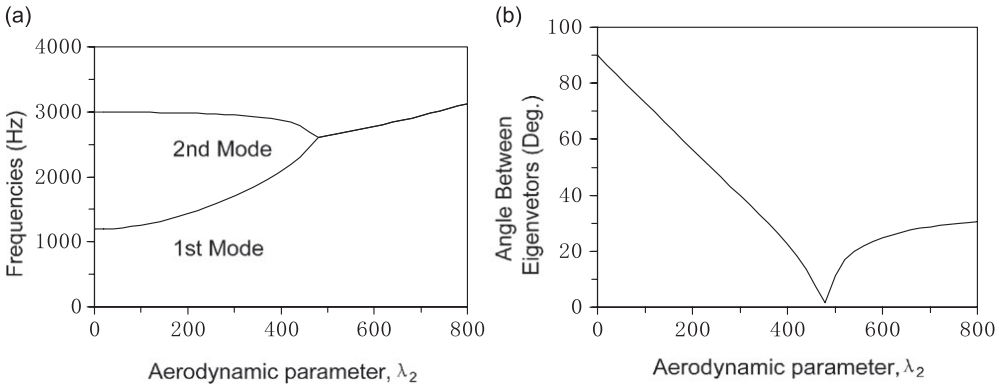

Fig. 6. Flutter prediction of the simply supported plate by using both methods: (a) coalescence of eigenvalues and (b) eigenvector orientation.

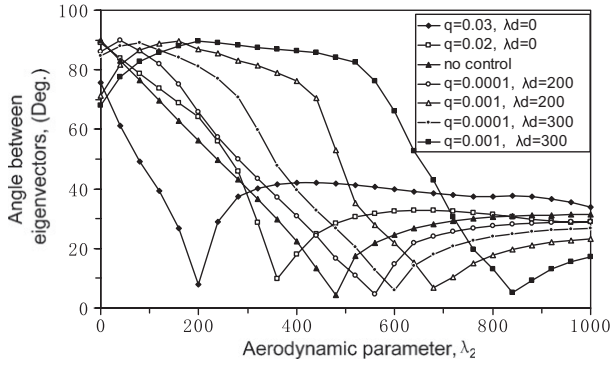

Fig. 7. Angle between the two lowest modes with control moments on all 16 elements.

Table 4
Flutter speed for different combinations of control parameters q and λ_d with control moments applied on all 16 elements.

Controller parameters		Critical flutter speed, λ_{cr}
λ_d	q	
0	0.03	200
0	0.02	360
Uncontrolled case		480
200	0.0001	560
200	0.001	680
300	0.0001	600
300	0.001	840

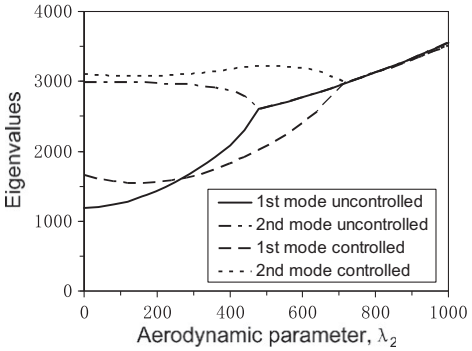

Fig. 8. Eigenvaues for $q=0.001$ and $\lambda_d=200$ with control moments on all 16 elements.

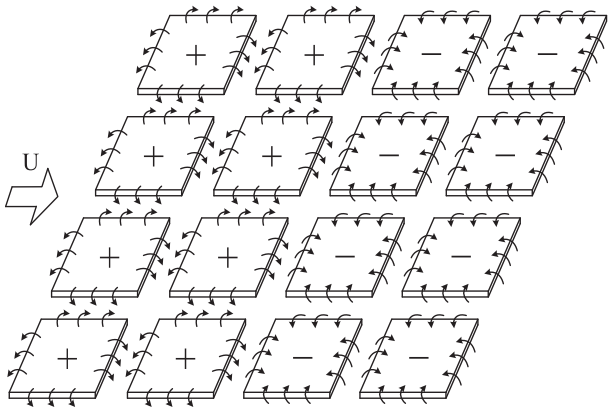

Fig. 9. The configuration of specific control moment combinations at $\lambda_2=240$ with $q=0.001$ and $\lambda_d=200$.

flutter speeds cannot be increased above $\lambda_{cr}=480$ (uncontrolled case). Once the control parameter λ_d is increased to 200 or 300, flutter speeds can be increased above the uncontrolled case at $\lambda_{cr}=480$. In both cases, flutter speeds seem to increase as the control parameter q increases. It is opposite of that observed for the case when $\lambda_d=0$.

The eigenvalues for the lowest two modes are plotted in Fig. 8 for the uncontrolled case and a specific case with $q=0.001$ and $\lambda_d=200$. It is seen that the lowest two eigenvalues coalesce and become complex at $\lambda_{cr}=480$ and 680, indicating the onset of flutter in the two, respectively, cases. The effect of the piezoelectric actuator increases the critical aerodynamic pressure due to the application of controlled bending moments to move the flutter speed to that of a higher flutter speed.

Fig. 9 shows a specific control moment combinations at $\lambda_2=240$ with $q=0.001$ and $\lambda_d=200$. Depending on the actual deflections and slopes of all nodes, controller is designed to determine the necessary change $\Delta\mathbf{S}$ in the system matrix to stabilize the system. This $\Delta\mathbf{S}$ can then be used to calculate the direction and magnitude of the external control moments, which are needed to be applied at the appropriate edges of each element.

The corresponding modes shapes for the uncontrolled case and specific case are shown in Fig. 10 for four specific values of λ_2 from zero to 680. For the uncontrolled case, it is seen that the first mode is dominated by a bending mode and the second mode is mainly dominated by a torsion mode at $\lambda_2=0$, indicating stability. As aerodynamic pressure is increased from zero, the first mode keeps the original modality, but the maximum deflection point moves from the center of plate along the direction of airflow while the second mode gradually loses its torsion dominant modality under the effect of airflow. Finally, the lowest two modes become similar at $\lambda_{cr}=480$, indicating the onset of flutter.

When the control moments are added, it can be seen that the lowest two controlled mode shapes are still distinct at $\lambda_2=480$, as well as in all other values below $\lambda_{cr}=680$, indicating stability. This interesting phenomenon indicates that the critical aerodynamic pressure λ_{cr} is increased from 480 to 680 by using the piezoelectric actuators.

5.2.2. Case 2: Applying control moments on the eight end elements

When the control moments are assumed to be applied on the eight end elements (elements 1, 2, 3, 4, 13, 14, 15 and 16 in Fig. 1b), flutter speed can again be both decreased and increased depending on the controller design. This concept is illustrated in Fig. 11. It can be seen that a series of combinations of control parameters q and λ_d are used to obtain seven critical flutter speeds varying from $\lambda_{cr}=240$ to 800 including the uncontrolled case of $\lambda_{cr}=480$.

Once again, all critical flutter speeds, control parameters q and λ_d are listed in Table 5 for simplicity. The same trends can be seen as in the case when the control moments are assumed to be applied on all 16 elements: For $\lambda_d=0$, flutter speed increases as the control parameter q decreases, whereas for $\lambda_d=200$ or 300 flutter speed increases as the control parameter q increases. Flutter speed can be increased above $\lambda_{cr}=480$ only when $\lambda_d=200$ or 300. However, for this example studied, the range of flutter speed variation changes less than the case 1 with the same control parameters q and λ_d, which may mean that the actual control effect declined when the control moments are applied on the eight end elements.

The eigenvalues for the lowest two modes are plotted in Fig. 12 for the uncontrolled case and a specific case with $q=0.0001$ and $\lambda_d=300$. It can be seen that the lowest two eigenvalues, respectively, coalesce and become complex at $\lambda_{cr}=480$ for the uncontrolled case and $\lambda_{cr}=560$ for the specific controlled case, indicating the onset of flutter. The corresponding mode shapes are shown in Fig. 13. Similar to the case when control moments are applied to all 16 elements, the lowest two mode shapes become similar at $\lambda_{cr}=480$ for the uncontrolled case and $\lambda_{cr}=560$ for the specific controlled

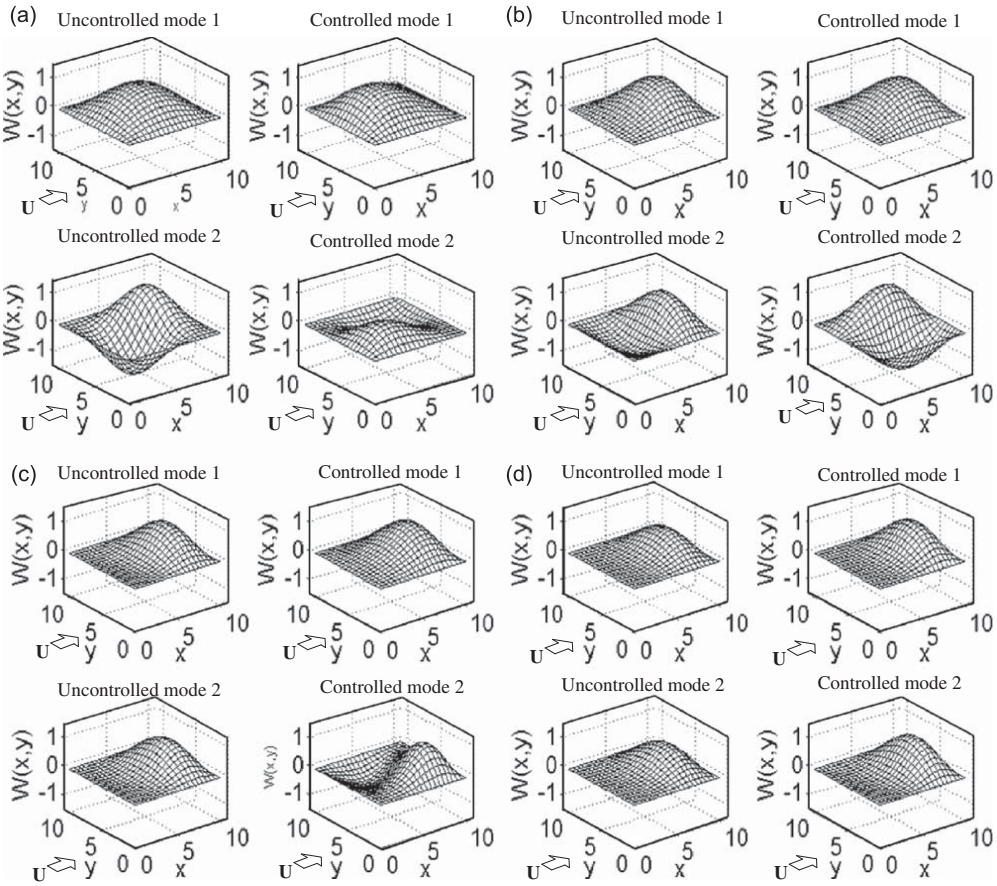

Fig. 10. Mode shapes for $q=0.001$ and $\lambda_d=200$ with control moments on all 16 elements at (a) $\lambda_2=0$; (b)$\lambda_2=240$; (c) $\lambda_2=480$; and (d) $\lambda_2=680$.

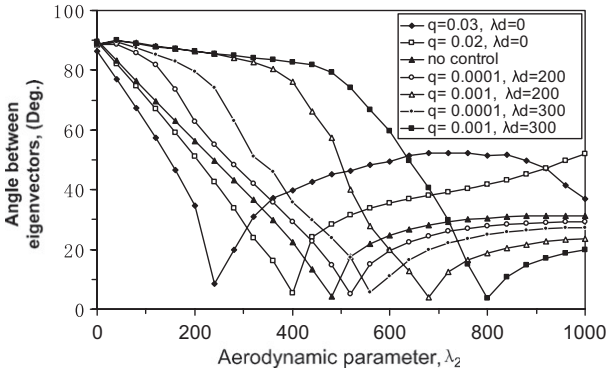

Fig. 11. Angle between the lowest two modes with control moments on eight end elements.

Table 5
Flutter speed for different combinations of control parameters q and λ_d with control moments applied on eight end elements.

Controller parameters		Critical flutter speed, λ_{cr}
λ_d	q	
0	0.03	240
0	0.02	400
Uncontrolled case		480
200	0.0001	520
200	0.001	680
300	0.0001	560
300	0.001	800

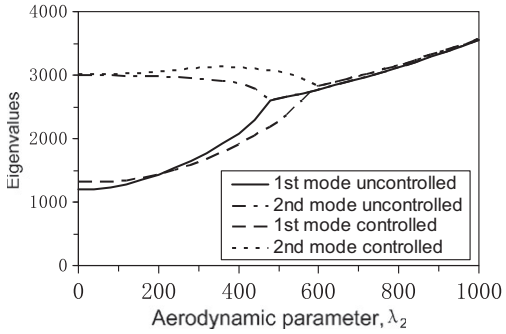

Fig. 12. Eigenvalues for and with control moments on $q=0.0001$ and $\lambda_d=300$ eight end elements.

case, indicating the onset of flutter. The presence of the piezoelectric actuators increases the critical aerodynamic pressure due to the effect of the added stiffness produced by the application of controlled bending moments to cause the two lowest modes no longer coalesce or the angle between them vanish.

5.2.3. Case 3: Applying control moments on the eight interior elements

Assuming that the control bending moments are only applied on the eight interior elements (elements 5, 6, 7, 8, 9, 10, 11, and 12 in Fig. 1b), flutter speed can again be both decreased and increased depending on the controller design. This concept is illustrated in Fig. 14. It can be seen that a series of combinations of control parameter q and λ_d are used to obtain seven critical flutter speeds varying from $\lambda_{cr}=400$ to 760 including the uncontrolled case of $\lambda_{cr}=480$.

Once again, all critical flutter speeds, control parameters q and λ_d are listed in Table 6. The same trends can be seen as in the previous two cases: for $\lambda_d=0$, flutter speed increases as the control parameter q decreases, whereas for $\lambda_d=200$ or 300 flutter speed increases as the control parameter q increases. Flutter speed can be increased above $\lambda_{cr}=480$ only when $\lambda_d=200$ or 300. However, for this example studied, the range of flutter speed variation is the smallest in this three cases

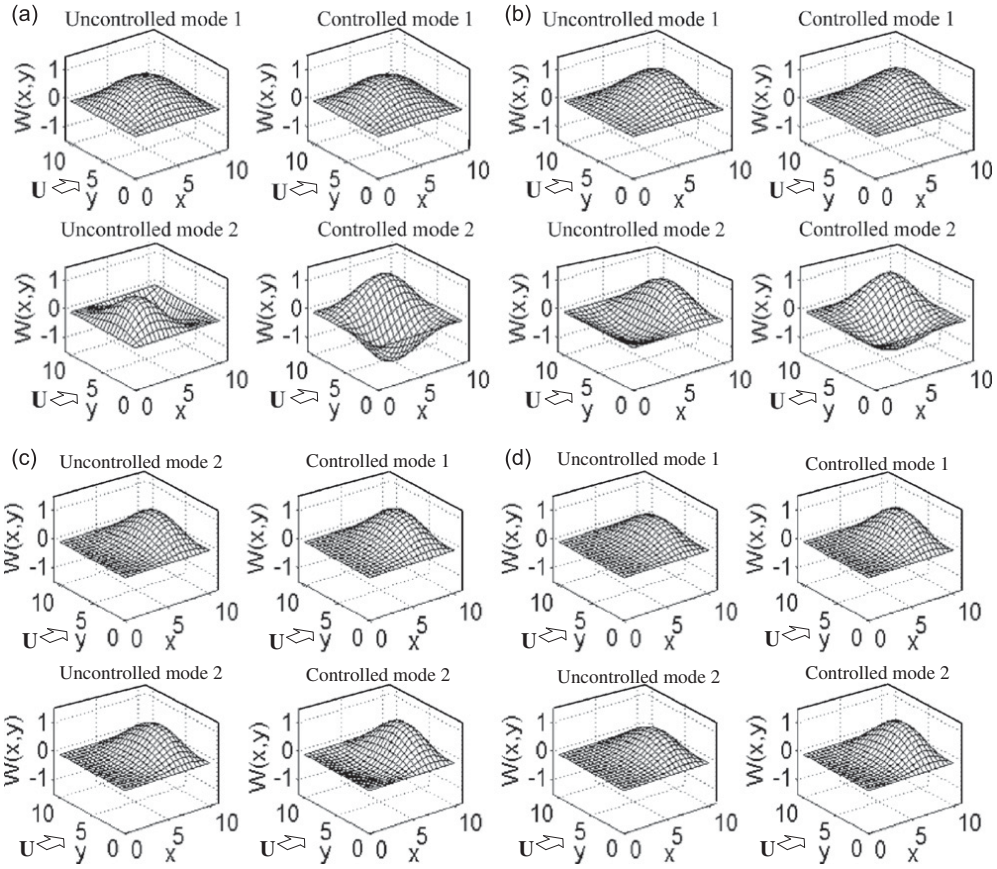

Fig. 13. Mode shapes for $q=0.0001$ and $\lambda_d=300$ with control moments on eight end elements at (a) $\lambda_2=0$; (b) $\lambda_2=240$; (c) $\lambda_2=480$; and (d) $\lambda_2=560$.

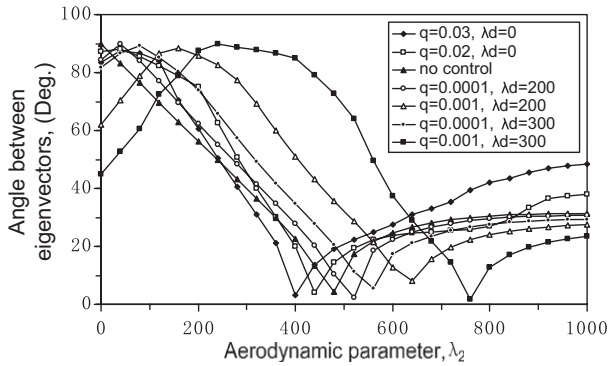

Fig. 14. Angle between the lowest two modes with control moments on eight interior elements.

with the same control parameters q and λ_d, which means that the actual control effect is the least when the control moments are applied on the eight interior elements.

The eigenvalues for the lowest two modes are plotted in Fig. 15 for the uncontrolled case and a specific case with $q=0.001$ and $\lambda_d=200$. It can be seen that the lowest two eigenvalues, respectively, coalesce and become complex at $\lambda_{cr}=480$ for the uncontrolled case and $\lambda_{cr}=640$ for the specific controlled case, indicating the onset of flutter. The corresponding mode shapes are shown in Fig. 16. Similar to the case when control moments are applied at all 16 elements, the lowest two mode shapes become similar at $\lambda_{cr}=480$ for the uncontrolled case and $\lambda_{cr}=640$ for the specific controlled case, indicating the onset of flutter. The presence of the piezoelectric actuators increases the critical aerodynamic pressure due to the effect of the added stiffness produced by the application of controlled bending moments to cause the two lowest modes no longer coalesce or the angle between them vanish.

Table 6
Flutter speed for different combinations of control parameters q and λ_d with control moments applied on eight interior elements.

Controller parameters		Critical flutter speed, λ_{cr}
λ_d	q	
0	0.03	400
0	0.02	440
Uncontrolled case		480
200	0.0001	520
200	0.001	560
300	0.0001	640
300	0.001	760

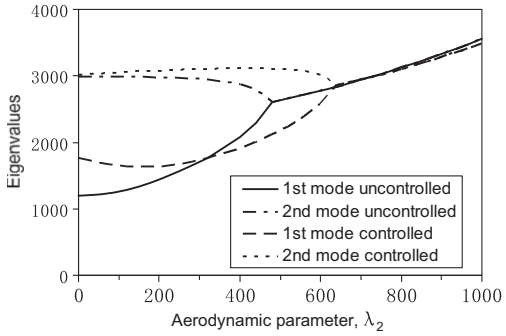

Fig. 15. Eigenvalues for $q=0.001$ and $\lambda_d=200$ with control moments on eight interior elements.

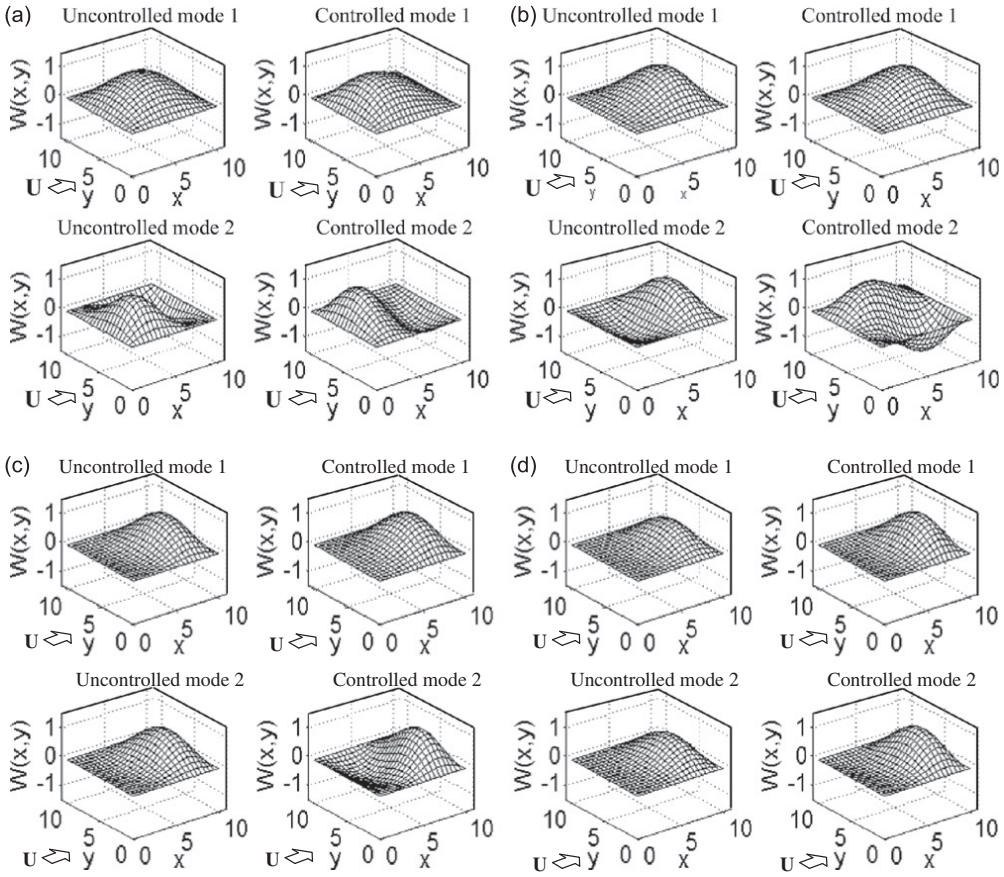

Fig. 16. Mode shapes for $q=0.0001$ and $\lambda_d=200$ with control moments on eight interior elements at (a) $\lambda_2=0$; (b) $\lambda_2=240$; (c) $\lambda_2=480$; and (d) $\lambda_2=640$.

6. Concluding remarks

A method of flutter detection and suppression using the eigenvector orientation approach and piezoelectric layers has been developed. The linear optimal control design is based on linear quadratic regulator theory and the nonlinear modal equations of motions. For the example of rectangular plate, the performance of flutter suppression using piezoelectric actuation is demonstrated by changing the piezoelectric actuator locations and the control parameters q and λ_d.

Considering only the three specific examples studied here, it is observed that when the control moments applied on all 16 sub-components of the panel, the flutter speed appears to be increased a little more than when applying the control moment on only eight end or eight interior sub-components. The phenomena observed seems to be due to the differences in added bending stiffness in suppressing the vibration modes to avoid the coalescence of the two lowest modes or to avoid the angle between them to vanish. Results seem to reveal that using control moments on more elements seems to be more effective in moving the flutter boundary to a higher speed.

It should be noted that there are several limitations as to offsetting the flutter speed in each case. One limitation is that each controller can only achieve a certain amount of increase in the flutter speed. Another limitation is the power needed from the piezoelectric layers, which is determined by the amplitude of the structural vibration as shown in Eq. (15). By using different controller design to optimize the limitation, the critical aerodynamic pressure parameter can be increased about two times, which reveals the great potential of piezoelectric materials to suppress flutter. While the demonstration of the usefulness of the current methods appear to be simple, straightforward, yet original for a two dimensional panel, its potential for application in aeronautical wing-type structures can be developed into an innovative technology, especially in view of the fact that the eigenvector method may provide a precious "lead time" necessary to activate control to suppress the destructive flutter.

References

[1] R.L. Bisplinghoff, H. Ashley, *Principles of Aeroelasticity*, Dover, New York, 1962.
[2] E.H. Dowell, *Aeroelasticity of Plates and Shells*, Noordhoff International, Leyden, The Netherlands, 1975.
[3] Y.C. Fung, *An Introduction to the Theory of Aeroelasticity*, John Wiley & Sons Inc., New York, 1955.
[4] E.I. Garrick, W.H. Reed, Historical development of aircraft flutter, *Journal of Aircraft* 18 (1) (1981) 897–912.
[5] R.M.V. Pidaparti, T.Y. Yang, Supersonic flutter analysis of composite plates and shells, *AIAA Journal* 31 (6) (1993) 1109–1117.
[6] M.D. Olson, Finite elements applied to panel flutter, *AIAA Journal* 5 (12) (1967) 2267–2270.
[7] M.D. Olson, Some flutter solutions using finite elements, *AIAA Journal* 8 (4) (1970) 747–752.
[8] A.D. Han, T.Y. Yang, Nonlinear panel flutter using high-order triangular finite elements, *AIAA Journal* 21 (10) (1983) 1453–1461.
[9] T.Y. Yang, Flutter of flat finite element panels in a supersonic potential glow, *AIAA Journal* 13 (11) (1975) 1502–1507.
[10] T.Y. Yang, S.H. Sung, Finite element panel flutter in three-dimensional supersonic unsteady potential flow, *AIAA Journal* 15 (12) (1977) 1677–1683.
[11] D. Afolabi, R.M.V. Pidaparti, H.T.Y. Yang, Flutter prediction using an eigenvector orientation approach, *AIAA Journal* 36 (1) (1998) 69–74.
[12] E.F. Crawley, J.D. Luis, Use of piezoelectric actuators as elements of intelligent structures, *AIAA Journal* 25 (10) (1987) 1373–1385.
[13] R.M.V. Pidaparti, V.A. Tischler, V.B. Venkayya, Flutter prediction methods for aeroelastic design optimization, *Journal of Aircraft* 38 (3) (2001) 557–559.
[14] R.C. Scott, T.A. Weisshaar, Controlling panel flutter using adaptive materials, *Journal of Aircraft* 31 (1) (1994) 213–222.
[15] R.C. Zhou, Z.H. Lai, D.Y. Xue, J.K. Huang, C. Mei, Suppression of nonlinear panel flutter with piezoelectric actuators using finite element method, *AIAA Journal* 33 (6) (1995) 1098–1105.
[16] E.E. Forster, H.T.Y. Yang, Flutter control of wing boxes using piezoelectric actuators, *Journal of Aircraft* 35 (6) (1998) 949–957.
[17] N. Sebastijanovic, T.W. Ma, H.T.Y. Yang, Panel flutter detection and control using eigenvector orientation and piezoelectric layers, *AIAA Journal* 45 (1) (2006) 118–127.
[18] J.-H. Han, J. Tani, J. Qiu, Active flutter suppression of a lifting surface using piezoelectric actuation and modern control theory, *Journal of Sound and Vibration* 291 (3) (2006) 706–722.
[19] A. Adini, Analysis of Plate Bending Using Triangular Elements, PhD Thesis, University of California at Berkeley, 1961.
[20] F.K. Bogner, R.L. Fox, L.A. Schmit Jr., The generation of interelement-compatible stiffness and mass matrices by the use of interpolation formulas, *Conference on Matrix Methods in Structural Mechanics*, Fairborn, OH, 1966, pp. 397–444.
[21] T.Y. Yang, *Finite Element Structural Analysis*, Prentice-Hall, New Jersey, 1986.
[22] IEEE Standard on Piezoelectricity, American National Standards Institute/IEEE Standard, 176–1987, New York, 1988.
[23] E.H. Dowell, Panel flutter—a review of the aeroelastic stability of plates and shells, *AIAA Journal* 8 (3) (1970) 385–399.
[24] B. Friedland, *Control System Design*, McGraw-Hill, New York, 1986.